Cell Flexibility Affects the Alignment of Model Myxobacteria

Albertas Janulevicius,[†*] Mark C. M. van Loosdrecht,[†] Angelo Simone,[‡] and Cristian Picioreanu[†]
[†]Environmental Biotechnology Group, Department of Biotechnology, and [‡]Faculty of Civil Engineering and Geosciences, Delft University of Technology, Delft, The Netherlands

ABSTRACT Myxobacteria are social bacteria that exhibit a complex life cycle culminating in the development of multicellular fruiting bodies. The alignment of rod-shaped myxobacteria cells within populations is crucial for development to proceed. It has been suggested that myxobacteria align due to mechanical interactions between gliding cells and that cell flexibility facilitates reorientation of cells upon mechanical contact. However, these suggestions have not been based on experimental or theoretical evidence. Here we created a computational mass-spring model of a flexible rod-shaped cell that glides on a substratum periodically reversing direction. The model was formulated in terms of experimentally measurable mechanical parameters, such as engine force, bending stiffness, and drag coefficient. We investigated how cell flexibility and motility engine type affected the pattern of cell gliding and the alignment of a population of 500 mechanically interacting cells. It was found that a flexible cell powered by engine force at the rear of the cell, as suggested by the slime extrusion hypothesis for myxobacteria motility engine, would not be able to glide in the direction of its long axis. A population of rigid reversing cells could indeed align due to mechanical interactions between cells, but cell flexibility impaired the alignment.

INTRODUCTION

Myxobacteria are social bacteria that exhibit a complex life cycle. When nutrients are available, myxobacteria cooperatively swarm and feed. Upon starvation, they aggregate to form multicellular spore-filled fruiting bodies, whose structure in different species can vary from simple mounds to elaborate treelike structures (1,2). Although significant insight into the morphogenesis of myxobacterial fruiting bodies has been made over the recent decades, mechanisms of their formation are not completely understood.

Swarming of myxobacteria and the formation of fruiting bodies depend on the movement of individual cells. Myxobacteria cells are flexible rods (3,4) that move on a substratum by gliding, which is defined as the movement of a bacterium on a solid surface in the direction of the long axis of the cell without the aid of flagella (5). Two gliding motility systems have been identified in *Myxococcus xanthus,* the most studied myxobacterium (6). One type of motility, S-motility, is known to be powered by the extension, adhesion, and retraction of type IV pili from the leading pole of the cell (7). The other type, A-motility, is less understood. Two dominant hypotheses for A-motility suggest that it might be powered by extrusion of slime from the rear of the cell (the slime-gun model, (8)) or alternatively, by focal adhesion complexes that are fixed to the substratum along the whole length of the cell (9), similar to focal adhesions of eukaryotic cells (10). Myxobacterial cells periodically reverse the direction of gliding, i.e., the leading pole after the reversal becomes the trailing pole (11).

Throughout their life cycle, multiple myxobacteria cells often align to form rafts, sheets, spirals, streams, and traveling waves (ripples) (12–17). Swarms and fruiting bodies are also formed by domains of aligned cells (12,18). It has been shown that alignment of *M. xanthus* cells is necessary for development of fruiting bodies to proceed, because it allows for transfer of membrane-bound C-signal, an essential regulator of *M. xanthus* development (19). Organized arrays of aligned cells can form from initially randomly oriented cells within several hours (13,20). It is known that A-motility alone is sufficient for domains of aligned cells to form (20), but mechanisms of cell alignment are not known. It has been suggested that myxobacteria align due to mechanical interactions between moving rod-shaped cells (20–22), and that cell flexibility facilitates reorientation of cells upon mechanical contact (23,24). However, these suggestions have not been based on experimental or theoretical evidence.

Numerous modeling studies addressed the question of myxobacterial development (22,25,26), but only a few of them studied the importance of mechanical factors. It has been shown that stiff rods can locally align because of geometrical constraints (27), and that a population of self-propelled stiff rods can form clusters due to mechanical interactions (28). In another study (29), a cellular Potts model was used to show that cell flexibility affects cell clustering in a population of 100 nonreversing cells, but no prediction of measurable bending stiffness values was made. In this article, by means of a computational mass-spring model, we study how the movement of a single flexible rod-shaped cell and the alignment of a population of 500 mechanically interacting cells depend on cell flexibility and A-motility engine type. The model is formulated in terms of experimentally measurable mechanical parameters, such as engine force, bending stiffness, and drag coefficient. We consider two A-motility hypotheses that correspond to

Submitted March 28, 2010 and accepted for publication August 27, 2010.

*Correspondence: a.janulevicius@tudelft.nl

Editor: Alexander Mogilner.

0006-3495/10/11/3129/10 $2.00

doi: 10.1016/j.bpj.2010.08.075

the slime-gun and the focal adhesions models. The results of the study reveal the importance of cell bending stiffness on the gliding pattern of a slime-gun powered cell and on the ability of a larger population of cells to align.

MODEL DESCRIPTION

To study the pattern of cell gliding and the alignment of a population of cells, we created a mass-spring model (30) of a flexible rod-shaped bacterium that moves on a substratum and interacts mechanically with other bacteria. In the model description that follows, we represent vectors by boldface letters and magnitudes of the vectors by the same lightface letters.

Particles

A bacterium of length L and width W is modeled as an ordered array of N particles that are connected by linear and angular springs (Fig. 1 *A*). Every particle $i = 1,\ldots,N$ has a position $\boldsymbol{r}_i$, velocity $\boldsymbol{v}_i$, and is acted upon by various forces $\boldsymbol{F}_i$. Forces that act on a particle arise from linear and angular springs within the same bacterium, an engine that propels the bacterium, drag with the substratum, and collisions between different bacteria or parts of the same bacterium.

Linear springs

Linear springs keep adjacent particles of the same bacterium at a certain distance apart, resisting elongation or shortening of the bacterium (Fig. 1 *B*). A linear spring i connects every two adjacent particles i and $i+1$, and is defined by a vector $\boldsymbol{l}_i = \boldsymbol{r}_{i+1} - \boldsymbol{r}_i$, where $i = 1,\ldots,N-1$ and l_i is the length of the spring, an equilibrium length $l_0 = (L-W)/(N-1)$ and a stiffness k^l. The force exerted by the linear spring i on particle i is determined by Hooke's law,

$$\boldsymbol{F}_i^{l,i} = -k^l(l_i - l_0)(\boldsymbol{l}_i/l_i).$$

The same linear spring i exerts an opposite force

$$\boldsymbol{F}_{i+1}^{l,i} = -\boldsymbol{F}_i^{l,i}$$

on the adjacent particle $i+1$. Moving and colliding myxobacteria cells do not shorten or elongate (31), therefore, the value of k^l was chosen to be large enough to model a cell that does not change its length markedly during simulations (Table 1).

Angular springs

Angular springs allow a bacterium to resist bending. An angular spring i connects every three adjacent particles i, $i+1$ and $i+2$, where $i = 1,\ldots,N-2$ (Fig. 1 *C*). The angular spring i has a stiffness k^a and exerts forces on all three particles so that the angle α_i between $\boldsymbol{l}_i$ and $\boldsymbol{l}_{i+1}$ decreases. When the three particles are aligned, i.e., when $\alpha_i = 0$, the angular spring does not exert any forces. The angular spring i produces two self-equilibrating torques with respect to $\boldsymbol{r}_{i+1}$: a torque $\boldsymbol{\tau}_i^{a,i}$ on particle i and a torque $\boldsymbol{\tau}_{i+2}^{a,i}$ on particle $i+2$. The magnitude of both torques is $\tau^{a,i} = k^a\alpha_i$, the direction of $\boldsymbol{\tau}_i^{a,i}$ is $\hat{\boldsymbol{\tau}}_i^{a,i} = \boldsymbol{m}_i/m_i$, where $\boldsymbol{m}_i = \boldsymbol{l}_i \times \boldsymbol{l}_{i+1}$, and the direction of $\boldsymbol{\tau}_{i+2}^{a,i}$ is $\hat{\boldsymbol{\tau}}_{i+2}^{a,i} = -\hat{\boldsymbol{\tau}}_i^{a,i}$.

The respective forces on the particles are

$$\boldsymbol{F}_i^{a,i} = \left(\tau^{a,i}/l_i^2\right)\left(\boldsymbol{l}_i \times \hat{\boldsymbol{\tau}}_i^{a,i}\right),$$
$$\boldsymbol{F}_{i+2}^{a,i} = -\left(\tau^{a,i}/l_{i+1}^2\right)\left(\boldsymbol{l}_{i+1} \times \hat{\boldsymbol{\tau}}_{i+2}^{a,i}\right),$$
$$\boldsymbol{F}_{i+1}^{a,i} = -(\boldsymbol{F}_i^{a,i} + \boldsymbol{F}_{i+2}^{a,i}).$$

The system of three particles acted by an angular spring defined in this way satisfies the conservation of linear and angular momenta.

Engine forces

Because S-motility is not necessary for the alignment of *M. xanthus* cells (20), we model only A-motility. Two

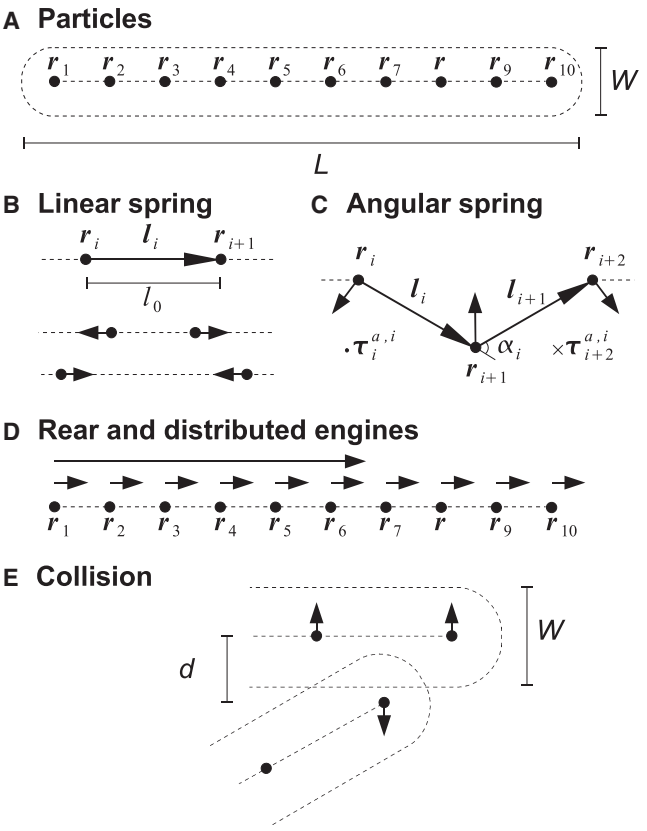

FIGURE 1 A mass-spring model of a flexible rod-shaped cell. Arrows without notation represent forces on particles. See text for explanation. (*A*) A bacterium of length L and width W comprised of $N = 10$ particles at positions $\boldsymbol{r}_1$, $\boldsymbol{r}_2$, …, $\boldsymbol{r}_{10}$. (*B*) A linear spring i and the forces it produces on particles i and $i+1$. (*C*) An angular spring i and the forces it produces on particles i, $i+1$ and $i+2$. (*D*) Rear and distributed engine forces in a bacterium with $N = 10$ and $k^e = -1$. (*E*) An example of forces of collision between two bacteria.

TABLE 1 Parameter values used for simulations

Parameter	Value	Description
Model		
L	5 μm	Length of bacterium (25)
W	0.5 μm	Width of bacterium (25)
ρ	1000 kg/m^3	Density of bacterium (approximately equal to the density of water)
N	10	Number of particles per bacterium
k^l	10^{-2} N/m	Stiffness of a linear spring
k^a	10^{-15}–10^{-18} N·m	Range of angular spring stiffnesses studied
k^c	6×10^{-4} N/m	Stiffness of collision
F^e	100 pN	Engine force (8)
v_b	4 μm/min	Speed of bacterial gliding (25)
T_R average	8.8 min	Average reversal time (25)
T_R standard deviation	2.1 min	Standard deviation of reversal time (25)
Solver		
atol	2.5×10^{-10} m	Absolute error tolerance*

*An integration step is successful when error does not exceed *atol* (35).

different A-motility hypotheses are introduced in the model:

1. A distributed engine (analogous to the focal adhesions hypothesis), where a force is generated along the whole length of the cell, and
2. A rear engine (analogous to the slime-gun hypothesis), where a force is generated at the trailing pole of the cell.

Because a bacterium can reverse its direction of movement, an engine direction property k^e determines which pole of the bacterium is the leading or the trailing pole. k^e can take values -1 or 1; if $k^e = 1$, the particle $i = 1$ is the leading pole and the particle $i = N$ is the trailing pole, whereas $k^e = -1$ indicates the opposite case. The reversal of direction is modeled as a change in the value of k^e. Further, at every particle position $\boldsymbol{r}_i$ we define a unit vector $\hat{\boldsymbol{t}}_i$ tangent to the bacterial body. The value $\hat{\boldsymbol{t}}_i$ has the same direction as $-k^e(\boldsymbol{l}_{i-1} + \boldsymbol{l}_i)$, if $i = 2,\ldots,N-1$, the direction of $-k^e\boldsymbol{l}_i$ if $i = 1$ and the direction of $-k^e\boldsymbol{l}_{i-1}$ if $i = N$. The distributed engine is then modeled by adding to every particle i of the bacterium a force

$$\boldsymbol{F}_i^e = (F^e/N)\hat{\boldsymbol{t}}_i,$$

where F^e is the magnitude of the engine force (Table 1), whereas a rear engine is modeled by adding a force

$$\boldsymbol{F}_i^e = F^e\hat{\boldsymbol{t}}_i$$

to the trailing particle of the bacterium (Fig. 1 *D*). The magnitude of the A-motility engine force is unknown; we use the value obtained by theoretical estimation of Wolgemuth et al. (8) (see Table 1). We also investigate how a change in the magnitude of the engine force affects the outcome of simulations.

Collision detection and response

A number of bacteria moving on a substratum or parts of a bending bacterium can overlap, resulting in a collision. In such an event, we introduce forces that separate bacteria or their parts (Fig. 1 *E*). For collision detection and response, a bacterium $j = 1, \ldots, M$, where M is the number of bacteria in the population, is viewed as an array of line segments, whose ends are defined by particle positions. Each ith line segment of a bacterium j is defined parametrically by $\boldsymbol{Q}_{ij}(P) = \boldsymbol{r}_{ij} + P(\boldsymbol{r}_{(i+1)j} - \boldsymbol{r}_{ij})$, where $0 \le P \le 1$ and $\boldsymbol{r}_{ij}$ indicates the position of a particle i in a bacterium j. If two line segments $\boldsymbol{Q}_{ij}$ and $\boldsymbol{Q}_{kl}$ are not adjacent segments on the same bacterium (i.e., if the segments do not share the same endpoint), a collision occurs if the distance between them becomes smaller than the bacterial width W. Thus, for each such pair of segments we find the points $\boldsymbol{Q}_{ij}(P_1)$ and $\boldsymbol{Q}_{kl}(P_2)$ on those segments that are separated by the smallest distance d, where $\boldsymbol{d} = \boldsymbol{Q}_{ij}(P_1) - \boldsymbol{Q}_{kl}(P_2)$ (32). If $d < W$, we introduce interaction forces to the particles at the ends of the segments to push the two segments apart:

$$\begin{aligned}
\boldsymbol{F}_{ij}^c &= -(1-P_1)[k^c(d-W)(\boldsymbol{d}/d)],\\
\boldsymbol{F}_{(i+1)j}^c &= -P_1[k^c(d-W)(\boldsymbol{d}/d)],\\
\boldsymbol{F}_{kl}^c &= (1-P_2)[k^c(d-W)(\boldsymbol{d}/d)],\\
\boldsymbol{F}_{(k+1)l}^c &= P_2[k^c(d-W)(\boldsymbol{d}/d)],
\end{aligned}$$

where k^c is the collision stiffness. Parameter k^c is chosen freely to ensure that moving bacteria or parts of the same bacterium do not overlap markedly during the simulation (Table 1).

In addition, excessive bending of each angular spring i is limited by introducing interaction forces on particles $\boldsymbol{r}_i$ and $\boldsymbol{r}_{i+2}$. Because the length of a segment in our simulations does not effectively change due to stiff linear springs, the forces are introduced if the distance between the particles $\boldsymbol{r}_i$ and $\boldsymbol{r}_{i+2}$ become smaller than W, i.e., we find a vector $\boldsymbol{d} = \boldsymbol{r}_i - \boldsymbol{r}_{i+2}$ and introduce forces

$$\begin{aligned}
\boldsymbol{F}_i^c &= -k^c(d-W)(\boldsymbol{d}/d),\\
\boldsymbol{F}_{i+2}^c &= k^c(d-W)(\boldsymbol{d}/d)
\end{aligned}$$

if $d < W$.

Drag forces and equations of motion

A myxobacterium on a substratum will often move in slime that is secreted by the cell itself and by other cells (33). A bacterium moving at relatively slow speeds in viscous slime (i.e., at low Reynolds numbers) will be acted upon by Stokes drag force that is proportional to velocity of the bacterium. As predicted by the slender body theory, drag force on a cylinder-shaped myxobacterium would be twice

as large in the direction normal to the bacterial body compared to the drag force in the direction parallel to the body (34). We model this effect by considering anisotropic Stokes drag forces on separate particles. The direction tangential to the bacterium body is $\hat{\boldsymbol{t}}_i$ (see Engine Forces, above), and the direction normal to bacterial body is $\hat{\boldsymbol{n}}_i$, found by rotating $\hat{\boldsymbol{t}}_i$ by $\pi/2$ in the plane made by $\boldsymbol{l}_i$ and $\boldsymbol{l}_{i+1}$. The drag force on a particle i in the direction tangent to the bacterial body is

$$\boldsymbol{F}_i^{d,t} = -\zeta^t \boldsymbol{v}_i^t,$$

and the drag force in the direction normal to bacterial body is

$$\boldsymbol{F}_i^{d,n} = -\zeta^n \boldsymbol{v}_i^n,$$

where superscripts t and n denote component vectors and a drag coefficient ζ in the direction of $\hat{\boldsymbol{t}}_i$ and $\hat{\boldsymbol{n}}_i$, respectively. The terminal (final) velocity of a particle, $\boldsymbol{v}^f{}_i$, is the velocity at which the drag force will balance all the other forces acting on the particle,

$$\begin{aligned}\boldsymbol{v}_i^f = \boldsymbol{v}_i^{f,t} + \boldsymbol{v}_i^{f,n} &= (1/\zeta^t)\boldsymbol{F}_i^t + (1/\zeta^n)\boldsymbol{F}_i^n \\ &= (1/\zeta^t)(\hat{\boldsymbol{t}}_i \cdot \boldsymbol{F}_i)\hat{\boldsymbol{t}}_i + (1/\zeta^n)(\hat{\boldsymbol{n}}_i \cdot \boldsymbol{F}_i)\hat{\boldsymbol{n}}_i\,,\end{aligned}$$

where $\boldsymbol{F}_i$ is the sum of the forces of all linear and angular springs, engine and contact forces that act on a particle i,

$$\boldsymbol{F}_i = \boldsymbol{F}_i^l + \boldsymbol{F}_i^a + \boldsymbol{F}_i^e + \boldsymbol{F}_i^c,$$

and $\zeta^n = 2\zeta^t$.

To our knowledge, the drag coefficient of a myxobacterium moving on a substratum has not been experimentally determined. Therefore, the value of ζ^t was chosen so that the terminal speed of a model bacterium powered by the engine force and moving in a straight line would be equal to the experimentally observed speed of *M. xanthus* v_b (Table 1), resulting in $\zeta^t = (F^e/N)/v_b$. Given the values of F^e and v_b, mass of a particle $m = \rho L\pi(W/2)^2/N$, found by approximating the shape of a bacterium by a cylinder with density ρ (Table 1), the value of ζ^t was found to be such that the bacterium reaches the terminal velocity in $\sim 10^{-11}$s. Because the timescale of myxobacteria movement is that of minutes, we assume in the model that inertia effects are negligible and that the velocity of a particle at each given time is $\boldsymbol{v}_i = \boldsymbol{v}^f{}_i$, proportional to the sum of forces that act on it (excluding drag). This leads to a system of differential equations

$$\frac{d\boldsymbol{r}_i(t)}{dt} = \boldsymbol{v}_i^f(t) \qquad (1)$$

for all bacteria j, describing the movement of all particles of all bacteria in the population.

In this study, all bacteria move on a planar substratum (i.e., on the x-y plane). Therefore vectors $\boldsymbol{r}_i$ and $\boldsymbol{v}_i$ are two-dimensional and the system in Eq. 1 translates into a system of $2 \times N \times M$ ordinary differential equations. We solve the system numerically with the Dormand-Prince fifth-order Runge-Kutta method (35) to obtain the positions of all particles in time. The algorithm was modified to include a maximum time step $W/(4v_b)$ in order to allow for collision detection. The parameter values used for simulations and error tolerance of the solver are listed in Table 1.

After each successful integration step, the direction of a bacterium is reversed if $t - t_{LR} > T_R$, where t is the current time of the simulation, t_{LR} is the time of the last reversal of the bacterium, and T_R is time interval until the next reversal. After a reversal, a new T_R value for the bacterium is sampled from a normal distribution with parameters following experimental measurements by Wu et al. (25).

Analysis of results

Every value of k_a was mapped to bending stiffness B of a bacterium viewed as a beam using the following procedure. A model bacterium was fixed at one end, a known force normal to the bacterial body was applied to the free end, and its deflection was calculated. Bending stiffness was then found from $B = (F/\Delta z)((L - W)^3/3)$, where F is the magnitude of the applied force and Δz is the deflection of the free end (36).

The orientation of a bacterium j was defined as a vector pointing from the trailing particle to the leading particle of the bacterium, $\boldsymbol{o}_j = k_e(\boldsymbol{r}_{1j} - \boldsymbol{r}_{Nj})$.

Alignment of a population of cells at time t was quantified by average orientation correlation (similar to the orientation correlation function used by Wu et al. (25)),

$$C(t) = (1/K)\sum\nolimits_{j \neq k}^{K}\left[2\cos^2\theta\left(\boldsymbol{o}_j(t), \boldsymbol{o}_k(t)\right) - 1\right],$$

where the sum is over all cell pairs, K is the number of cell pairs, and $\theta(\boldsymbol{o}_j(t), \boldsymbol{o}_k(t))$ is the angle between the orientations of bacteria j and k at time t. Each term in the sum is equal to 1 if the two cells are aligned and equal to -1 if the orientations of the two cells are perpendicular. The ability of a cell j to maintain its orientation in time was quantified by the orientation autocorrelation function,

$$C_j^a(\Delta t) = (1/K)\sum_t\left[2\cos^2\theta\left(\boldsymbol{o}_j(t), \boldsymbol{o}_j(t + \Delta t)\right) - 1\right],$$

where the sum is over all t values for which $t + \Delta t$ are defined, and K is the number of such values. This function shows how well the orientation of the cell at time t is correlated with its orientation at time $t + \Delta t$.

RESULTS

In this study, we investigated how flexibility of a rod-shaped cell affected:

1. The pattern of movement of a single cell powered by the rear and distributed engines.

2. The alignment of two colliding cells.
3. The alignment of a population of 500 mechanically interacting cells.

Flexible rear-engine powered cells exhibit flailing behavior

We first modeled gliding of a single cell on a substratum and studied how bending stiffness of the cell and the engine type affected the pattern of cell movement. The cell was initially placed with all its particles in a straight line, except for the trailing particle, which was offset from the long axis of the cell by 1% of cell width to introduce initial perturbation in engine direction. Cells with the distributed engine moved in a straight line independently of their bending stiffness (see Movie S1 in the Supporting Material). However, rear-powered cells moved in a straight line only for large bending stiffness values. For small bending stiffness values, shortly after the movement started, cells exhibited flailing behavior, i.e., complex snakelike movements (see Fig. 2, Movie S2, and Movie S3) that were a result of cell bending caused by the engine force acting on the trailing pole of the cell. Very flexible cells with the rear engine were completely unable to produce directed movement (Movie S3). In a flailing cell, the trailing particle travels a longer distance than the leading particle. This observation allowed us to estimate that the bending stiffness value below which a rear-engine cell exhibited flailing was $B_f = 2 \times 10^{-23}$ J·m (Fig. S1 *A*). In general, the value of B_f depends on the size of the engine force: a larger force is able to bend stiffer cells and is therefore expected to result in a larger value of B_f (Fig. S1).

Two flexible cells align better upon contact than two rigid cells

We next simulated a collision between two nonreversing cells and estimated how cell alignment after the collision depends on cell bending stiffness and the engine type. Two cells were initially placed on a substratum with random orientations and with their leading particles at random positions in a square with side L. Movements of the two cells were then simulated over an interval of 5 min. We studied a number of random initial configurations, each determined by initial positions and orientations of the cells. For each configuration we simulated movements of the cells for different bending stiffness values and two engine types. An

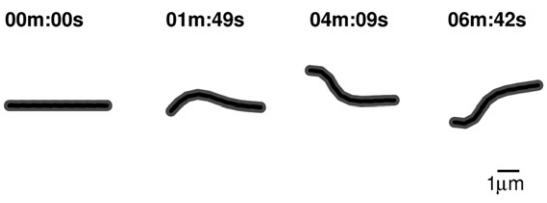

FIGURE 2 Shape and position of a rear-powered flailing cell at different times ($B = 1.2 \times 10^{-23}$ J·m).

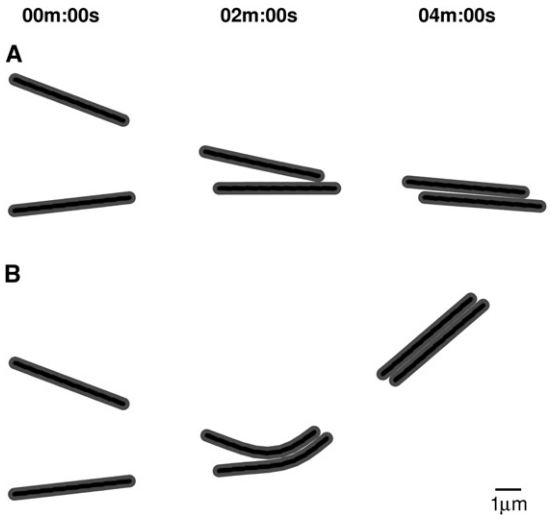

FIGURE 3 Positions and shapes of two colliding cells with distributed engine at different times. In panels *A* and *B*, cells start from the same initial configuration. (*A*) Rigid cells, $B = 6.1 \times 10^{-22}$ J·m. (*B*) Flexible cells, $B = 7.0 \times 10^{-25}$ J·m.

example of the two cell collisions for two different bending stiffness values is shown in Fig. 3, Movie S4 and Movie S5.

We analyzed only those initial configurations that resulted in an effective collision between cells, i.e., the configurations where a collision between distributed engine cells produced a change in orientation of 5° or more of at least one cell for at least one bending stiffness value. For cells with the distributed engine, the average alignment of the two cells due to collision increased as the bending stiffness of the cell decreased (Fig. 4, *solid line*). The alignment of rear-powered cells due to collision depended on cell flexibility in a similar manner only above the value B_f (Fig. 4, *dashed line*). Below B_f, rear-engine cells exhibited flailing behavior, continuously changed their orientation and therefore their ability to align was impaired. These results suggest that for nonflailing cells, flexibility helps two colliding cells to align. Similar results are obtained with different magnitudes of the engine force (Fig. S2).

Flexibility interferes with the alignment of a population of cells

The effect of cell flexibility on the alignment of a large population of cells was interestingly found to be opposite of that on the alignment of two colliding cells. We simulated movements of 500 reversing, mechanically interacting cells over a period of 4 h and studied how the alignment of the population is affected by bending stiffness of the cell. The 500 cells were initially placed in a square computational domain with random positions and orientations (Fig. 5 *A*). The size of the domain was chosen so that the density of cells was $1/(\pi(L/2)^2) = 5 \times 10^6$ cm^{-2}. This density value allows for random distribution of cells within the domain and is physiologically relevant (37). Periodic boundaries

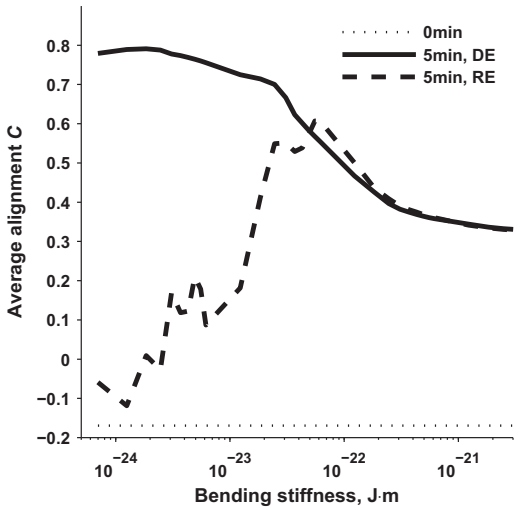

FIGURE 4 Average alignment C of two cells as a function of cell bending stiffness before the collision (*dotted line*), at 5 min for distributed-engine cells (*DE*, *solid line*), at 5 min for rear-engine cells (*RE*, *dashed line*). For each bending stiffness value, alignment C was averaged over 188 different initial configurations. Initial average alignment (*dotted line*) is negative because the initial configurations where the cells were well aligned did not produce effective collisions and were removed from the analysis (see text).

of the domain ensured that a (part of) bacterium leaving the domain entered it from the opposite side, keeping the density of bacteria in the domain constant.

Simulation results show that populations of rigid cells are well aligned at 4 h (Fig. 5 *B*) and the alignment is relatively stable (see Fig. S3 and Movie S6). In contrast, populations of flexible cells appear poorly aligned, although small temporary clusters consisting of tens of aligned cells are still visible (Fig. 5 *C*, Fig. S3, and Movie S7). The alignment (average orientation correlation) of a population at 4 h for different cell bending stiffness values and two engine types is shown in Fig. 6 (see also Fig. S4 for variability between individual simulations). The average orientation correlation is close to zero (i.e., alignment is poor) for small bending stiffness values, but increases steeply to a plateau value as bending stiffness of the cell increases. In other words, flexibility impairs the ability of a population to align for cells both with the distributed and the rear engines. Below the bending stiffness value B_f a population of rear-powered cells is not expected to align well due to cell flailing, as the simulation results confirm (Fig. 6). However, a population of rear-powered cells shows poor alignment for bending stiffness values as high as 7×10^{-23} J·m, the values for which a rear-powered cell does not flail. This suggests that flexibility interferes with the alignment of rear-powered cells directly, but not through the effect on the flailing motion of the cell.

We also found that the effect of cell flexibility on the alignment of the population is robust with respect to the initial configuration of cells. If all cells were initially aligned (Fig. S5 *A*), they remained well aligned throughout the 4 h if the cells were rigid (Fig. S5 *B*). However, a population of flexible cells rapidly lost its alignment (Fig. S5 *C* and Movie S8). The average orientation correlation of a population at 4 h as a function of the bending stiffness of the cell has a similar appearance to the one shown in Fig. 6 (Fig. S6).

In addition, to show that the effect of cell flexibility on the ability of a population to remain aligned is robust with respect to cell density in the domain, we simulated movements of 490 densely-packed (cell density 4×10^7 cm^{-2}), initially aligned cells (Fig. 7 *A*). A population of rigid cells remained well aligned at 4 h (Fig.7 *B* and Movie S9), but a population of flexible cells lost their alignment (Fig.7 *C*, Movie S10, and Fig. S7).

Flexible cells are less likely to retain their orientation upon contact

To understand why the population of flexible cells is unable to align, although flexibility helps two colliding cells to align (Fig. 4), we analyzed the ability of a cell to retain its

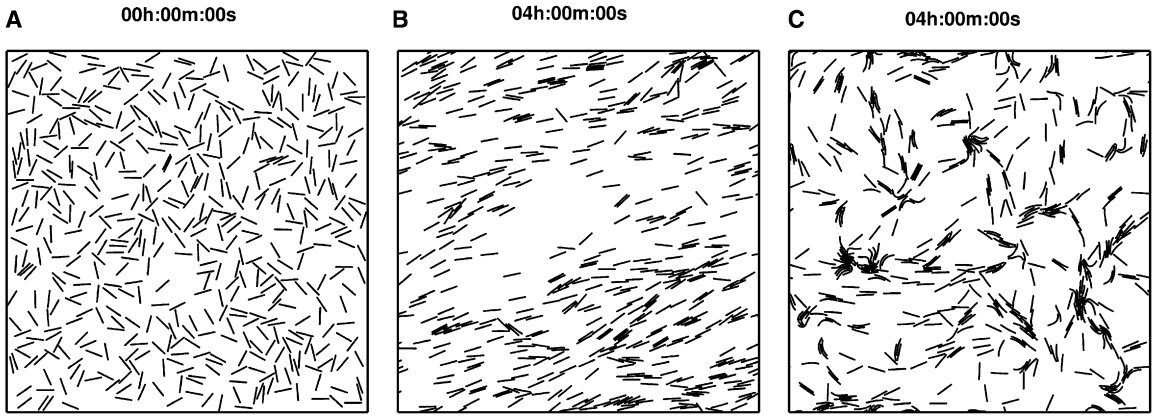

FIGURE 5 Spatial distribution of a population of 500 cells with the distributed engine at 0 h (*A*) and 4 h (*B* and *C*). Initially, the cells have random positions and orientations. The size of the domain is 100 μm, cell density in the domain is 5×10^6 cm^{-2}. (*B*) Rigid cells ($B = 6.1 \times 10^{-22}$ J·m). (*C*) Flexible cells ($B = 1.2 \times 10^{-23}$ J·m).

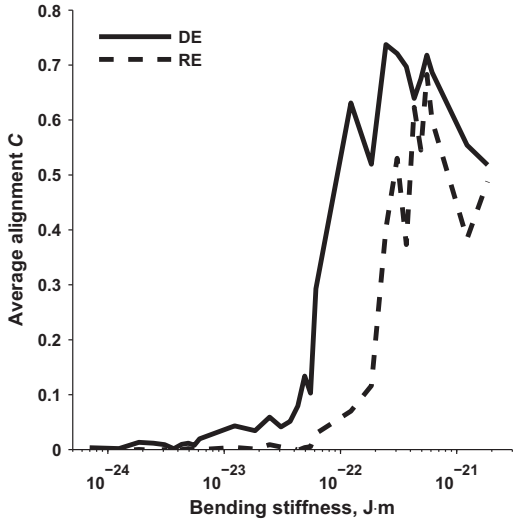

FIGURE 6 Alignment (average orientation correlation C) of a population at 4 h as a function of cell bending stiffness in the simulations where cells initially have random positions and orientations (Fig. 6). For each bending stiffness value, results of three simulations with different initial configurations of cells were averaged. (*Solid line*) Cells with distributed engine (*DE*), (*dashed line*) cells with rear engine (*RE*).

orientation during multiple contacts with other cells in the population. For rigid cells, the orientation autocorrelation function C^a, that shows how well orientations of a cell at different time intervals are correlated (see Analysis of results), maintains positive values for up to 4 h, the length of the simulation. However, when cells are flexible, the values of C^a decay to nearly zero for time intervals larger than ~15 min (Fig. 8 *A*). Fig. 8 *B* shows that the decay time of C^a increases with increasing bending stiffness. In other words, as a cell becomes more flexible, it loses the ability to maintain its orientation for longer times. Conversely, rigid cells are more resistant to changes in their orientation upon mechanical interaction with other cells.

Fig. 3 illustrates the mechanism of the inability of flexible cells to maintain their orientations upon contact. When two rigid cells that are almost aligned collide, they often adjust their orientations and continue to move in the directions similar to those before the contact (Fig. 3 *A* and Movie S4). However, if the cells are flexible, they bend upon contact and move in circular paths (Fig. 3 *B* and Movie S5). In both cases, cells align well; however, circular motion of flexible cells results in large changes in their orientations during the collision.

The inability of flexible cells to maintain their orientations upon contact can explain why a larger population of flexible cells is not capable to align. In a well-aligned population of flexible cells, the cells would collide at small angles and would markedly change their orientation (similar to the situation in Fig. 3 *B*). The new orientations of the two cells would be very different from the dominant orientation of the remaining population. Thus, multiple collisions between flexible cells would result in the deterioration of alignment of an initially aligned population (Movie S8 and Movie S10). Collisions between rigid cells in a well-aligned population would not change their orientation markedly (Fig. 3 *A*), thus keeping a population well aligned (Movie S9). This is further supported by the fact that for intermediate bending stiffness values (5×10^{-23} to 5×10^{-22} J·m), both the alignment of the population of rear-powered cells and the ability of a rear-engine cell to maintain orientation are poorer than those of cells with the distributed engine (Fig. 6 and Fig. 8 *B*). Poorer ability of a rear-engine cell to maintain orientation in comparison with a distributed engine cell can be explained by a larger torque that is applied by the rear engine force to the bent cell, resulting in a faster cell rotation upon contact. Furthermore, an increase in the magnitude of the engine force results in larger bending stiffness values for which a population fails to align (Fig. S8). Larger engine forces are able to bend stiffer cells, therefore their ability to maintain orientation is impaired.

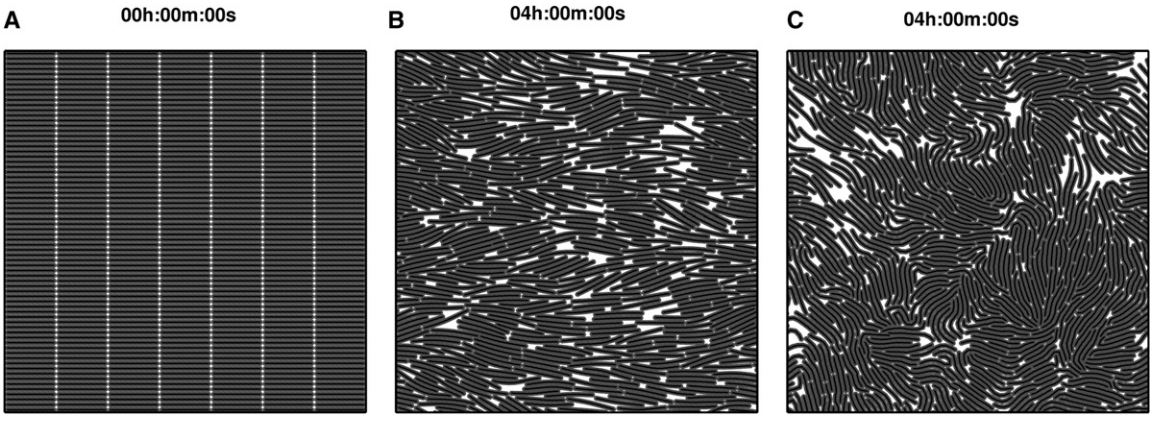

FIGURE 7 Spatial distribution of a population of 490 densely packed cells with the distributed engine at 0 h (*A*) and 4 h (*B* and *C*). Initially the cells are aligned. The size of the domain is 35 μm, cell density in the domain is 4×10^7 cm^{-2}. (*B*) Rigid cells ($B = 6.1 \times 10^{-22}$ J·m). (*C*) Flexible cells ($B = 1.2 \times 10^{-23}$ J·m).

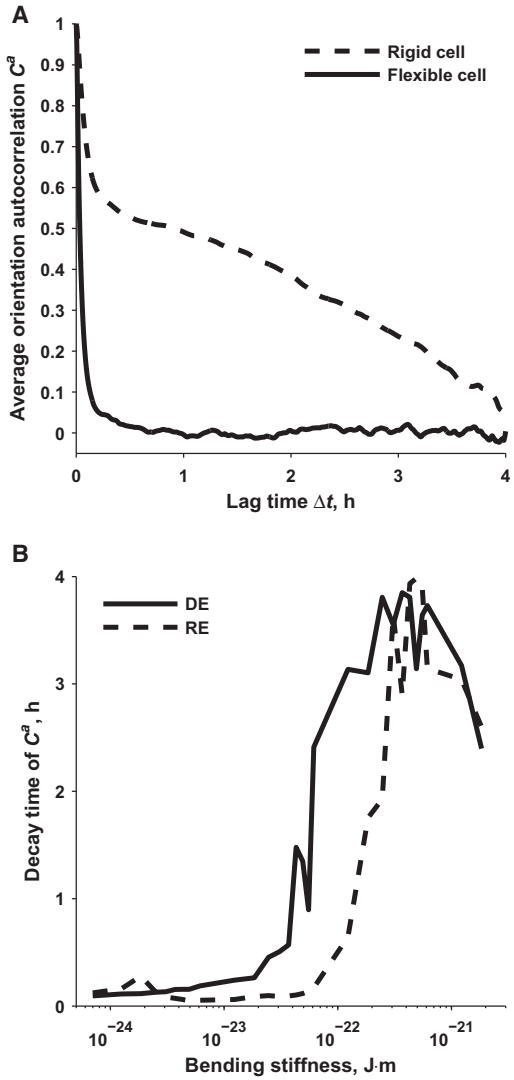

FIGURE 8 Ability of a cell to maintain its orientation upon mechanical interactions in a population of 500 cells with the distributed engine. Cell density in the domain is 5×10^6 cm^{-2}. (*A*) Average orientation autocorrelation function of flexible ($B = 1.2 \times 10^{-23}$ J·m) and rigid ($B = 6.1 \times 10^{-22}$ J·m) cells. (*B*) Decay time of average orientation autocorrelation function for different bending stiffness values. Decay time is defined as the time at which the orientation autocorrelation function value falls below 0.05. (*Solid line*) Cells with distributed engine (*DE*), (*dashed line*) cells with rear engine (*RE*).

DISCUSSION

In this study we created a mechanical mass-spring model of a flexible rod-shaped cell that glides on a substratum and showed that bending stiffness and engine type affected the pattern of cell gliding and the alignment of a population of 500 mechanically interacting cells.

Two motility systems have been described in *M. xanthus* (6). Whereas the mechanism of S-motility is known to involve the extension and retraction of type IV pili (7), the mechanism of A-motility is debated (38,39). Among the most discussed hypotheses for A-motility mechanism are the slime-gun model, where the force is generated at the trailing pole of the cell by extrusion and swelling of polyelectrolyte gel (8), and the focal adhesions model, where the force is produced at the sites of adhesion with the substratum along the whole length of the cell (9). Powered by the motility engine, a myxobacterium cell glides on a substratum along the long axis of the cell (31). Our simulations suggest that a rear-engine (i.e., slime-gun) powered cell would be able to travel in the direction of the long axis of the cell only when bending stiffness of the cell is above the value $B_f = 2 \times 10^{-23}$ J·m. Below that value, a cell would exhibit flailing, complex snakelike movements. Those movements would arise because the engine force acting on the trailing pole would bend the cell and produce torque that would rotate the cell. Flailing of *M. xanthus* has been observed experimentally when the leading pole of the cell is stuck (3,9). Our results show that a flexible rear-powered bacterium could exhibit flailing behavior even when the leading pole of a bacterium is free to move. Very flexible rear-engine cells would not be capable to produce any directed movement due to extensive flailing. In addition, we show that when engine forces are generated along the whole length of the cell, as the focal adhesions model of A-motility proposes, a cell would be able to glide along the long axis of the cell independently of its bending stiffness. To our knowledge, bending stiffness of a myxobacterium cell has not been experimentally determined. Wolgemuth (40) theoretically estimated bending stiffness of *M. xanthus* to be 3×10^{-23} J·m by using experimental observations of the shape of a flailing cell (3). Bending stiffness of a cell can also be estimated by assuming that the principal structural component of a cell is hollow-cylinder shaped cell wall. The bending stiffness can then be found from $B = \pi E a^3 t$, where E is Young's modulus of the cell wall, a is the radius of the cylinder, and t is the thickness of the cylinder wall (peptidoglycan) (36). Given the values of $E = 0.25$ MPa (41), $t = 6.35$ nm (*Escherichia coli*), and $t = 2.41$ nm (*Pseudomonas aeruginosa*) (42), bending stiffness of a *M. xanthus* cell is estimated to be between 3.0×10^{-23} J·m and 7.8×10^{-23} J·m. All estimated values are large enough to allow a slime-gun powered cell to produce directed movement, as predicted by our model. Furthermore, Kaiser and Crosby (14) observed that moving *M. xanthus* cells tend to glide with a small change in direction. In our model, such movement could be accounted for by a rear-engine powered cell with a bending stiffness value smaller but very close to B_f. It must also be emphasized that our determined value of B_f is dependent on the magnitude of the A-motility engine force, which has not been experimentally measured, but only estimated theoretically (8). To further investigate the conditions of cell flailing, the type of analysis performed by Wolgemuth (40) could also be appropriate.

Myxobacteria often form various multicellular structures from aligned cells, such as multicellular rafts, swirls, streams, or traveling waves (12–18). The extent of

alignment can vary from arrays of hundreds of aligned cells (13,18,20,25) to the global alignment of the whole population during traveling wave formation (16). It has been observed that a population of initially randomly oriented *M. xanthus* cells can form aligned domains within several hours (13,20), although mechanisms of cell alignment are not well known. It is often assumed that cells align due to mechanical interactions between cells (20–22) and that flexibility facilitates cell reorientation upon collision (24). Furthermore, slime trails that are left by gliding cells on a substratum and used by other gliding cells as tracks are thought to contribute to cell alignment (4,15,25,33). We show that a population of 500 randomly oriented reversing rigid cells (with bending stiffness values larger than 1×10^{-22} J·m for distributed engine cells and larger than 5×10^{-22} J·m for rear-engine cells), powered by A-motility alone, without the need of S-motility or slime trails, could align well within several hours only due to mechanical interactions between gliding cells. However, a population of flexible cells (with bending stiffness values smaller than 5×10^{-23} J·m) would not be able to align, but would only produce small temporary clusters consisting of tens of aligned cells. Because random orientations of cells at the beginning of development might only be a laboratory condition, hardly ever seen in nature (12), we also found that alignment or nonalignment of a population is robust with respect to the initial configuration of cells and cell density. In other words, a population of initially aligned flexible cells, even when they are densely packed, would not be able to maintain the aligned state, whereas a population of rigid cells would stay well aligned. The inability of a larger population of flexible cells to align in our simulations is caused by the tendency of flexible cells to bend upon contact and move in circular paths (Fig. 3 *B*), resulting in large changes in the orientations of colliding cells. In contrast, rigid cells are more resistant to changes in their orientation upon collision. The ability of colliding cells to align while maximally preserving their orientations before the contact appears to be crucial in order for a population to align or remain aligned in our model. Overall, we conclude that cell flexibility can interfere with the formation of streams, traveling waves, domains of aligned cells within swarms, or other structures from aligned cells.

Marked bending and movement of myxobacteria cells in circular paths while in contact have been observed experimentally at low cell densities (43), suggesting poor ability of myxobacteria cells to maintain their orientations upon collisions. In addition, for the bending stiffness value of a *M. xanthus* cell theoretically estimated by Wolgemuth (40), our model predicts that a population of cells would not be able to align within several hours only because of mechanical interactions between cells. We therefore suggest that other factors might play a role in the alignment of myxobacteria cells. Myxobacteria cells often move in slime secreted by other cells (33). Viscous extracellular slime surrounding cells could increase their effective bending stiffness, thus affecting their alignment and flailing behavior. It has also been proposed that focal adhesions (hypothesized to be a part of A-motility engine) may act as attachment points between a cell and substratum. A cell would have extra bending stiffness due to the attachment (44).

Kaiser and Welch (23) proposed that cell flexibility helps myxobacteria to overcome traffic jams during fruiting body formation. This idea is consistent with our findings that flexibility allows cells to more easily change orientation upon mechanical interaction. In addition, our results suggest that the value of bending stiffness of myxobacteria could be a result of a trade-off: the ability of a population to efficiently align (e.g., to form streams and traveling waves) at the initial stages of fruiting body development would require a rigid cell, whereas flexible cells would be preferable to overcome traffic-jams at later stages. Furthermore, myxobacteria cells might have evolved a mechanism to regulate their bending stiffness to serve for different purposes in the course of development. For example, the transition of myxobacteria from swarming, where cells are less aligned globally, to the rippling stage that shows a high degree of cell alignment could be a result of cell stiffening. Remarkably, cells of different species appear to have different flexibility (4), but the importance of this difference is unknown.

In conclusion, the proposed model shows that cell flexibility can be an important factor affecting both the movement of single myxobacteria cells and the alignment of cell populations. Experimental measurement of the important parameters of myxobacteria cells—bending stiffness, engine force, and drag with the substratum—will allow to make more-accurate predictions with the current model. In addition, our model does not consider possible cell-substratum binding forces due to focal adhesions. Although very little is known about the mechanics of focal adhesions, these binding forces could potentially affect cell collision dynamics. Furthermore, cells in our simulations move on a surface in a single layer, an assumption reasonable only for low density of cells. It would be important to investigate three-dimensional cell movement in multilayer populations.

SUPPORTING MATERIAL

Eight figures and 10 movies are available at http://www.biophysj.org/biophysj/supplemental/S0006-3495(10)01109-4.

Albertas Janulevicius thanks Jouke Heringa (Department of Radiation, Radionuclides and Reactors, Faculty of Applied Sciences, Delft University of Technology) for excellent technical support. Access to high performance computing resources made available by Igor Nikolic (Faculty of Technology, Policy and Management, Delft University of Technology) is gratefully acknowledged.

This study was funded by the Netherlands Organization for Scientific Research (VIDI grant No. 864-06-003).

REFERENCES

1. Kaiser, D. 2003. Coupling cell movement to multicellular development in myxobacteria. *Nat. Rev. Microbiol.* 1:45–54.
2. Shimkets, L. J., M. Dworkin, and H. Reichenbach. 2006. The myxobacteria. *In* The Prokaryotes. M. Dworkin, S. Falkow, E. Rosenberg, K. H. Schleifer, and E. Stackebrandt, editors. Springer, New York. 31–115.
3. Spormann, A. M., and A. D. Kaiser. 1995. Gliding movements in *Myxococcus xanthus*. *J. Bacteriol.* 177:5846–5852.
4. Reichenbach, H., H. H. Heunert, and H. Kuczka. 1965. Swarm development and morphogenesis by myxobacteria—*Archangium, Myxococcus, Chondrococcus, Chondromyces*. Institute for Scientific Film, Göttingen. Film C 893.
5. Henrichsen, J. 1972. Bacterial surface translocation: a survey and a classification. *Bacteriol. Rev.* 36:478–503.
6. Hodgkin, J., and D. Kaiser. 1979. Genetics of gliding motility in *Myxococcus xanthus* (*Myxobacterales*): two gene systems control movement. *Mol. Gen. Genet.* 171:177–191.
7. Sun, H., D. R. Zusman, and W. Shi. 2000. Type IV pilus of *Myxococcus xanthus* is a motility apparatus controlled by the *frz* chemosensory system. *Curr. Biol.* 10:1143–1146.
8. Wolgemuth, C., E. Hoiczyk, …, G. Oster. 2002. How myxobacteria glide. *Curr. Biol.* 12:369–377.
9. Mignot, T., J. W. Shaevitz, …, D. R. Zusman. 2007. Evidence that focal adhesion complexes power bacterial gliding motility. *Science* 315: 853–856.
10. Wozniak, M. A., K. Modzelewska, …, P. J. Keely. 2004. Focal adhesion regulation of cell behavior. *Biochim. Biophys. Acta.* 1692:103–119.
11. Blackhart, B. D., and D. R. Zusman. 1985. "Frizzy" genes of *Myxococcus xanthus* are involved in control of frequency of reversal of gliding motility. *Proc. Natl. Acad. Sci. USA.* 82:8767–8770.
12. O'Connor, K. A., and D. R. Zusman. 1989. Patterns of cellular interactions during fruiting-body formation in *Myxococcus xanthus*. *J. Bacteriol.* 171:6013–6024.
13. Jelsbak, L., and L. Søgaard-Andersen. 2003. Cell behavior and cell-cell communication during fruiting body morphogenesis in *Myxococcus xanthus*. *J. Microbiol. Methods.* 55:829–839.
14. Kaiser, D., and C. Crosby. 1983. Cell movement and its coordination in swarms of *Myxococcus xanthus*. *Cell Motil. Cytoskeleton.* 3:227–245.
15. Vasquez, G. M., F. Qualls, and D. White. 1985. Morphogenesis of *Stigmatella aurantiaca* fruiting bodies. *J. Bacteriol.* 163:515–521.
16. Sager, B., and D. Kaiser. 1994. Intercellular C-signaling and the traveling waves of *Myxococcus*. *Genes Dev.* 8:2793–2804.
17. Sliusarenko, O., J. Neu, …, G. Oster. 2006. Accordion waves in *Myxococcus xanthus*. *Proc. Natl. Acad. Sci. USA.* 103:1534–1539.
18. Pelling, A. E., Y. Li, …, J. K. Gimzewski. 2006. Self-organized and highly ordered domain structures within swarms of *Myxococcus xanthus*. *Cell Motil. Cytoskeleton.* 63:141–148.
19. Kim, S. K., and D. Kaiser. 1990. Cell alignment required in differentiation of *Myxococcus xanthus*. *Science* 249:926–928.
20. Wall, D., and D. Kaiser. 1998. Alignment enhances the cell-to-cell transfer of pilus phenotype. *Proc. Natl. Acad. Sci. USA.* 95:3054–3058.
21. Welch, R., and D. Kaiser. 2001. Cell behavior in traveling wave patterns of myxobacteria. *Proc. Natl. Acad. Sci. USA.* 98:14907–14912.
22. Sliusarenko, O., J. Chen, and G. Oster. 2006. From biochemistry to morphogenesis in myxobacteria. *Bull. Math. Biol.* 68:1039–1051.
23. Kaiser, D., and R. Welch. 2004. Dynamics of fruiting body morphogenesis. *J. Bacteriol.* 186:919–927.
24. Kaiser, D. 2007. Bacterial swarming: a re-examination of cell-movement patterns. *Curr. Biol.* 17:R561–R570.
25. Wu, Y., A. D. Kaiser, …, M. S. Alber. 2009. Periodic reversal of direction allows myxobacteria to swarm. *Proc. Natl. Acad. Sci. USA.* 106:1222–1227.
26. Igoshin, O. A., A. Mogilner, …, G. Oster. 2001. Pattern formation and traveling waves in myxobacteria: theory and modeling. *Proc. Natl. Acad. Sci. USA.* 98:14913–14918.
27. Csahók, Z., and A. Czirók. 1997. Hydrodynamics of bacterial motion. *Physica A.* 243:304–318.
28. Peruani, F., A. Deutsch, and M. Bär. 2006. Nonequilibrium clustering of self-propelled rods. *Phys. Rev. E.* 74:030904.
29. Starruss, J., T. Bley, …, A. Deutsch. 2007. A new mechanism for collective migration in *Myxococcus xanthus*. *J. Stat. Phys.* 128: 269–286.
30. Eberly, D. H., and K. Shoemake. 2003. Game Physics. Morgan Kaufmann Publishers, San Francisco, CA.
31. Reichenbach, H., H. H. Heunert and H. Kuczka. 1965. *Myxococcus* spp. (*Myxobacteriales*)—Swarm development and formation of protocysts. Institute for Scientific Film, Göttingen. Film E 778.
32. Ericson, C. 2005. Real-Time Collision Detection. Morgan Kaufmann Publishers, San Francisco.
33. Burchard, R. P. 1982. Trail following by gliding bacteria. *J. Bacteriol.* 152:495–501.
34. Keller, J. B., and S. I. Rubinow. 1976. Slender-body theory for slow viscous flow. *J. Fluid Mech.* 75:705–714.
35. Press, W. H., S. A. Teukolsky, …, B. P. Flannery. 2007. Numerical recipes. *In* The Art of Scientific Computing, 3rd edition, Cambridge University Press, Cambridge, UK.
36. Gere, J. M., and S. P. Timoshenko. 1984. Mechanics of Materials. Kent Publishing, New York.
37. Shimkets, L. J., and M. Dworkin. 1981. Excreted adenosine is a cell density signal for the initiation of fruiting body formation in *Myxococcus xanthus*. *Dev. Biol.* 84:51–60.
38. Mignot, T. 2007. The elusive engine in *Myxococcus xanthus* gliding motility. *Cell. Mol. Life Sci.* 64:2733–2745.
39. Kaiser, D. 2008. *Myxococcus*—from single-cell polarity to complex multicellular patterns. *Annu. Rev. Genet.* 42:109–130.
40. Wolgemuth, C. W. 2005. Force and flexibility of flailing myxobacteria. *Biophys. J.* 89:945–950.
41. Pelling, A. E., Y. Li, …, J. K. Gimzewski. 2005. Nanoscale visualization and characterization of *Myxococcus xanthus* cells with atomic force microscopy. *Proc. Natl. Acad. Sci. USA.* 102:6484–6489.
42. Matias, V. R. F., A. Al-Amoudi, …, T. J. Beveridge. 2003. Cryotransmission electron microscopy of frozen-hydrated sections of *Escherichia coli* and *Pseudomonas aeruginosa*. *J. Bacteriol.* 185:6112–6118.
43. Kühlwein, H., B. Schlicke, …, H. H. Heunert. 1971. *Polyangium fuscum* (*Myxobacteriales*)—Cyst formation and swarm development. Institute for Scientific Film, Göttingen. Film E 1582.
44. Kaiser, D. 2009. Are there lateral as well as polar engines for A-motile gliding in myxobacteria? *J. Bacteriol.* 191:5336–5341.